Journal of Nuclear Materials 382 (2008) 184–189

Contents lists available at ScienceDirect

Journal of Nuclear Materials

journal homepage: www.elsevier.com/locate/jnucmat

Influence of alloying elements on grain-growth in Zr(Fe) and Cu(Fe) thin-films under in situ ion-irradiation

D. Kaoumi [a,*], A.T. Motta [a], R.C. Birtcher [b]

[a] Department of Mechanical and Nuclear Engineering, The Pennsylvania State University, University Park, PA 16802, United States
[b] Materials Science Division, Argonne National Laboratory, IL 60439, United States

A B S T R A C T

Thin-films of Zr(Fe) and Cu(Fe) were ion-irradiated in situ in a transmission electron microscope to study the influence of alloying elements on grain-growth. These two systems are different in that Zr–Fe has a negative heat of mixing and Cu–Fe a positive heat of mixing. Irradiations conducted at temperatures of 20–573 K showed precipitation in Zr(Fe) but not in Cu(Fe). The grain sizes increased monotonically with fluence and in both cases the pure metal exhibited more grain-growth than the alloy. A more drastic reduction of grain-growth rate was observed in Zr(Fe) (where precipitate drag occurred) than in Cu–Fe (where only solute drag was available). Zr(Fe) samples were also subjected to 1 MeV electron irradiation but no grain-growth was observed. The results are discussed in terms of the mechanisms of grain-growth under irradiation.

1. Introduction

Two processes of microstructure evolution of polycrystalline materials under irradiation which have received considerable attention [1–9] are irradiation induced phase transformation and grain-growth. One of the problems in studying these processes is that the kinetics is not usually accessible to the experimentalist, and thus the mechanisms are difficult to determine. In this work we examine the microstructure evolution of supersaturated Zr(Fe) and Cu(Fe) solid-solutions under in situ ion-beam irradiation in the intermediate voltage electron microscope (IVEM) at Argonne National Laboratory [10]. The advantage of an in situ study is the possibility of directly observing the phenomenon and its kinetics so that the mechanism and driving force can be understood in detail.

The binary Zr–Fe alloy system has been the focus of a number of studies because of its technological importance especially in the nuclear industry where Fe-containing Zr alloys are used as fuel cladding material. Preliminary results of the study of irradiation induced phase transformation in thin-foils of Zr(Fe) irradiated with 500 keV Kr ions were presented in [11]; they are complemented here by 1 MeV electron irradiations. The Zr(Fe) system (negative heat of mixing) is compared to the Cu(Fe) system (positive heat of mixing), under similar ion-irradiation conditions. Irradiation induced grain-growth occurs concomitantly with irradiation induced phase transformations. In this paper, we report on the effect of alloying elements on ion-irradiation induced grain-growth. Also, the 1 MeV electron irradiations provide important information on the role of the damage structure (cascades vs. isolated defects) on the microstructure evolution under irradiation.

2. Experimental methods

2.1. Sample preparation

Supersaturated solid-solutions of Cu(Fe) and Zr(Fe) were co-sputter deposited onto NaCl substrates and onto Si wafers (for Rutherford backscattering spectroscopy (RBS) characterization) using a dual gun system at a base pressure of the order of 10^{-7} Torr at room temperature at the Materials Research Laboratory (MRL, Penn State University). The as-deposited thin-films were 80–90 nm thick. The specimens on NaCl substrates were floated on a de-ionized water–ethanol solution onto TEM copper grids, cleaned and dried before they were irradiated.

2.2. Characterization of the as-deposited thin-films

In both types of as-deposited films the only diffraction pattern seen corresponds to the structure of the matrix (Cu and α-Zr, respectively). Because of the rapidity of the effective quench during thin-film deposition, no second-phase is formed, although Rutherford backscattering (RBS) and energy dispersive spectroscopy (EDS) analysis confirms an iron content in the Zr–Fe and Cu–Fe films well beyond the solubility limit of Fe both in Zr and Cu. In fact, the solubility of Fe in Zr at room temperature is just a few ppm [12] and in the case of Cu–Fe, the two elements are reportedly immiscible in solid state. Thus, the thin-films were processed as supersaturated solid-solutions of Fe in α-Zr and Cu, respectively.

* Corresponding author.
E-mail address: dxk909@psu.edu (D. Kaoumi).

0022-3115/$ - see front matter © 2008 Elsevier B.V. All rights reserved.
doi:10.1016/j.jnucmat.2008.08.011

Because Cu and Fe have practically the same atomic size ($\sim 1.179 \times 10^{-23}$ cm^3) the solid-solution of Fe in Cu is most likely substitutional whereas in the case of Zr–Fe, the Fe solute atoms are twice as small as the Zr matrix atoms and occupy interstitial sites [13]. The measured lattice parameter for the Cu–Fe solid solution was close to the measured lattice parameter for the pure Cu thin-films, and to the value of the lattice parameter obtained from the powder diffraction file for pure fcc Cu. This is consistent with the idea that the Cu–Fe solid-solutions processed were of the substitutional type as suggested above. On the other hand the lattice parameters for the hcp Zr(Fe) thin-films are slightly bigger than the powder diffraction file values for pure α-Zr, although the c/a ratio is the same. This suggests that interstitial Fe atoms cause the increase in lattice parameter.

Fig. 1 shows a bright-field image and associated diffraction pattern for Zr–(4.4 at.%)Fe and Cu–3%Fe in the as-deposited state. These films were laterally homogeneous, and nanocrystalline, with an initial mean grain size between 10 and 15 nm. Similar microstructure was seen for the other Zr(Fe) compositions. The as-deposited films have an approximately equiaxed grain microstructure. Many Moiré fringes were visible, indicating the presence of more than one layer of grains. In the case of the as-deposited Zr–Fe films, the grains were preferentially oriented with the basal plane perpendicular to the foil surface, as indicated by the high 002 intensity in Fig. 1 (bottom right). This preferential grain orientation differs from that observed in previous experiments [14]. For the Cu–Fe films, the relative intensity of the diffracted rings was as expected for powder patterns of coarse-grained Cu with no preferential orientation. Overall, the intensity of the diffracted rings is even around their circumference, indicating no in-plane texture for either system.

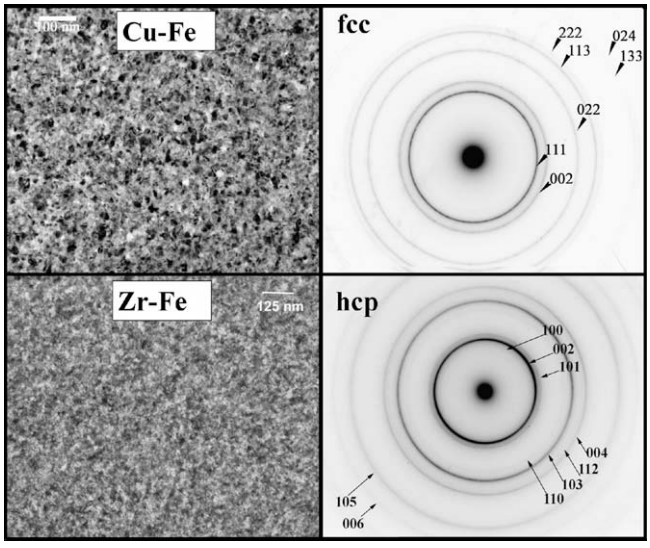

Fig. 1. Bright-fields and associated diffraction patterns of Cu–3%Fe and Zr–4.4%Fe films as deposited. The films are nanocrystalline with diffraction patterns characteristic of the pure metal: the rings of the Cu–Fe films were all indexed as fcc Cu rings and the rings of the Zr–Fe films were all indexed as hcp α-Zr rings.

3. Experiment

The thin-films were irradiated at the intermediate voltage electron microscope (IVEM)-TANDEM facility at Argonne National Laboratory, where an ion accelerator is attached to an electron microscope operated at 300 keV [10]. Samples were irradiated with 500 keV and 600 keV Kr^+ ions at fluxes typically around 2.50×10^{12} ions/cm^2 s to a fluence in excess of 10^{16} ions/cm^2 s, at temperatures ranging from 20 K to 573 K. The beam heating was calculated to be less than 10 K. This was verified by looking at the temperature rise upon turning on the beam (measured on a thermocouple placed at the specimen cup); this was typically only 2–3 K. The ion-beam energy was chosen on the basis of computer simulations using the Monte Carlo program SRIM2003 [15] so that ion-implantation is minimized in the films (ion ranges were 1700–2100 A). The evolution of the microstructure was followed by sequentially taking bright-field images and diffraction patterns (DP) of the films while they were being irradiated, which made it possible to follow the kinetics of the phenomena. Table 1 summarizes the experiments performed and the associated relevant irradiation-damage parameters obtained from SRIM2003. Grain-growth was studied by direct measurement of all the visible grains in bright-field micrographs, using an average of the long and small dimensions. The numbers of grains included varied from 30–40 per micrograph to 10–15 as the grain size increased.

The high voltage electron microscope at the Commissariat a l'Energie Atomique (CEA), (Saclay, France) was used to carry out 1-MeV-electron irradiations of Zr–Fe thin-films. The electron energy was 1 MeV, at a flux of $\sim 2.3 \times 10^{20}$ electron cm^{-2} s^{-1}. Using a displacement energy of 24 eV [16] we obtain 33 barn for the displacement cross section and a displacement a rate of $\sim 8.9 \times 10^{-3}$ dpa/s to and total doses up to 124 dpa.

It should be noted that in situ ion-irradiation of thin-foils brings some concerns, such as high dose rate, the possibility of the free surfaces of the foil acting as defect sinks, and sputtering. The first two simply indicate that the specific nature of the in situ ion-irradiation needs to be taken into account in the interpretation of the results [17] and the third was calculated using SRIM and appeared not to be significant for our irradiation conditions.

4. Results

4.1. Irradiation-enhanced phase transformation

4.1.1. The Zr–Fe system

4.1.1.1. Ion-irradiation. A previous study [11] revealed the formation of second-phase particles which were identified as body-centered tetragonal Zr_2Fe precipitates evenly distributed in the thin foil, at all irradiating temperatures above room temperature. Similar results were obtained in this study at all Fe compositions from 1.2% to 4.4%. According to the Zr–Fe equilibrium phase diagram

Table 1
Summary of the ion-irradiation conditions: melting points, ion type and energy, collisional properties, and irradiation temperature

Element	Melting point (K)	Ion type/ energy (keV)	Average deposited damage-energy F_D (eV/ion Å)	Average number of displacements/ion Å	Average displacement rate (dpa/s)	Irradiation temperature T_{irr} (K)
Cu–3%Fe	~1358	Kr 500	323	7.91	0.023	298, 473
Zr–1.2%Fe	~2128	Kr 500	194	3.25	0.019	298, 423, 573

The average deposited damage-energy F_D, displacements/ion/Å and displacement rate (dpa/s) were obtained from the SRIM2003 [13] Monte Carlo code using a displacement energy of 25 eV. For Cu(Fe) irradiated with 500 keV ions and Zr(Fe) irradiated with 500 keV Kr ions the collisional values for Cu and Zr were used.

[18], a mixture of this phase with α-Zr is thermodynamically metastable relative to the orthorhombic Zr_3Fe intermetallic phase in the range of temperatures and Fe content investigated. However the formation of Zr_2Fe still constitutes a net free energy decrease in the system relative to a solid solution of Fe in Zr. In fact, Zr_2Fe is often observed in melts of compositions where normally the orthorhombic Zr_3Fe phase (the most stable phase thermodynamically) is expected to be observed [19]. Also, studies of the crystallization of Zr–Fe glasses showed that the immediate products of crystallization are often metastable phases which would not have been predicted from the Zr–Fe phase diagram [20]. In situ annealing heat treatment in the absence of irradiation also caused precipitation of the Zr_2Fe intermetallic phase, but only above 673 K. An analogous process can occur in the inner regions of displacements cascades, where a sudden heating takes the material much above a nominal melting temperature. The maximum recoil energies in these experiments are greater than 100 keV, thus creating the possibility of dense cascades. The cooling of a dense cascade may be analogous then to a fast cooling from a melt, and Zr_2Fe again favored over Zr_3Fe.

Fig. 2 shows the bright-field micrographs of a Zr–1.2%Fe thin-film irradiated with 600 keV Kr ion-irradiation at 300 K and the corresponding diffraction patterns. The right-hand-side region was shadowed from the beam by a specimen grid and is therefore unirradiated, and the left-hand-side region was irradiated to a fluence of 10^{16} ion/cm^2 Kr ions. The diffraction pattern associated with the unirradiated area shows only the lines associated with the hcp phase present at the start of irradiation, while the diffraction pattern from the irradiated region shows new lines associated with the irradiation induced precipitates.

For all temperatures below 673 K, the precipitate formation occured solely within the irradiated area where displacement cascades occur. The kinetics of the irradiation-enhanced second-phase precipitation was followed by recording the diffraction patterns at regular intervals. The dose necessary for precipitation was found to decrease with increasing irradiation temperature indicating that the precipitation process is not a purely collisional process [11].

During ion-irradiation of Zr–Fe at 50 K, there is second-phase formation but the new phase was not identified. The pattern of rings formed (i.e. their ratio of d-spacings) suggests an fcc phase. Interestingly, at low temperature some amorphous intensity is visible, in parallel with the appearance of the crystalline rings corresponding to the new phase. The appearance of amorphous rings may indicate that at low temperature the mobility of the Fe atoms is not enough to make some of the amorphous intermetallic compound nuclei formed in cascades to grow into crystalline precipitates.

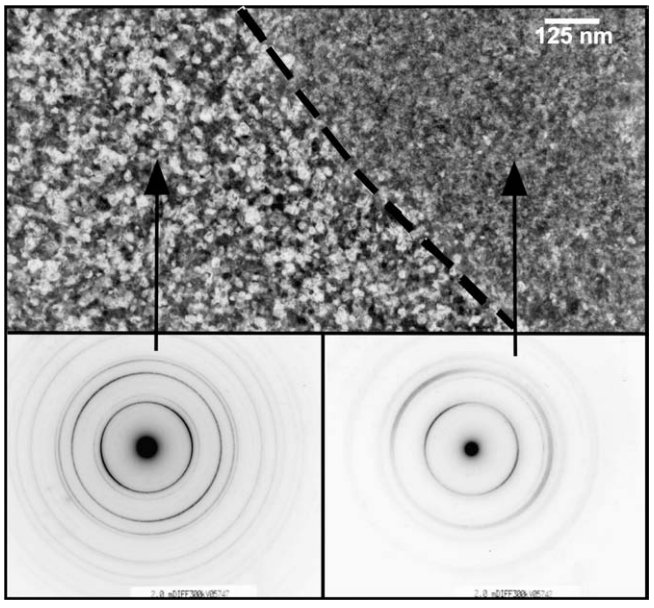

Fig. 2. Bright-field micrographs and corresponding diffraction patterns Zr–1.2%Fe sample irradiated at 300 K with 500 keV Kr ions (fluence of 10^{16} ions/cm^2), showing both the area hit by the beam (left) and the area shadowed by the grid.

4.1.1.2. Electron irradiation. Electron irradiation was conducted in order to help answer the question of whether the second-phase formation observed depends on the details of the damage structure or whether the transformation depends simply on the level of displacements per atom (dpa). Zr–Fe thin-foils were irradiated at room temperature to 124 dpa and at 573 K to 74 dpa.

In contrast with ion-irradiation, electron irradiation at room temperature and at 573 K did not enhance the Zr_2Fe precipitation. Towards the end of the irradiation time, some electron irradiation enhanced formation of zirconium oxide was observed in the 573 K irradiation. The EDS spectra clearly showed oxygen content in the irradiated area in larger proportion than in the non-irradiated area, likely caused by enhanced breakdown of carbohydrates and other molecules present in the vacuum of the TEM, occurring under the electron beam, as observed previously [21].

4.1.2. The Cu–Fe system

Solid-solutions of Cu supersaturated with 3 at.% Fe were irradiated with 500 keV Kr ions at 300 K and at 473 K. The irradiations at both temperatures showed no visible second-phase precipitation. Fig. 4 shows the bright-field image and diffraction pattern of the as-fabricated Cu–Fe thin-film (left) and the irradiated region at a final fluence of 10^{16} ions/cm^2, at 298 K (center), and 473 K (right), respectively. The diffraction patterns of the irradiated samples showed no extra ring when compared to the initial diffraction pattern but were spottier, revealing that grain-growth had occurred during irradiation, which was verified in the bright-field images.

In fact, the iron–copper system does not form intermetallic compounds and has negligible mutual solid solubility at temperatures below 973 K because of the large positive enthalpy of mixing ΔH_{mix} = +13 kJ mol^{-1} for an Fe–Cu system of 50 at.% Fe–50 at.% Cu [22], and therefore precipitation of Fe was expected. The fact that this did not occur in the Cu–Fe thin-films could be a result of the nature of the ion-irradiation induced damage. Indeed, it is considered that within the thermal spikes induced by ion-irradiation the local temperature can exceed the melting temperature so that the local regions are liquid-like. Although Cu and Fe are immiscible in solid state, they are miscible in the liquid state whereas Zr and Fe are miscible in both solid and liquid states). Thus, in Cu–Fe, the thermal-spike regions may actually enhance the mixing of Cu and Fe and prevent segregation of the Fe species. This thermal-spike effect was highlighted in ion-beam mixing experiments involving Cu/Fe and Ag/Fe bilayers [23]. Both systems are immiscible in solid state but contrary to Cu/Fe, Ag/Fe is still immiscible in liquid state. When irradiated with 2.5 MeV Au ions and 2 MeV Cu ions, ion-beam mixing was actually observed in the Cu/Fe system (and was larger than predicted by purely ballistic models), while no mixing was reported in the Ag/Fe system. The authors argued that ballistic atomic-mixing may occur in both cases during the collisional phase of the defect cascade formation. However, during the thermal-spike phase following the collisional phase in the cascade formation, Cu/Fe mixes further (in accordance with the thermodynamically miscibility of the system in the liquid state) while in the case of Ag/Fe, de-mixing occurs. The authors concluded that the experimental results, which resemble thermodynamically the liquid state, were in agreement with the assumption of atomic motion inside the thermal-spike in a liquid-like manner, which

supported the importance of atomic motion within the thermal-spike phase over both the early collisional phase of the cascade and over motion of radiation induced defects after the thermal-spike phase.

4.2. Irradiation induced grain-growth

In both Zr–Fe and Cu–Fe thin-films, direct observation of the films under ion-irradiation revealed a gradual increase of the average grain size (i.e. average grain diameter), at all irradiating temperatures, even at 20 K where thermal effects are negligible (grain-growth in these samples was studied under purely thermal conditions i.e., outside irradiation, and only found to occur above 873 K). The increase of grain size is apparent on the bright-field micrographs (Figs. 2 and 4 (top)) and on the diffraction patterns which became spottier as the fluence increased, indicating grain size increase.

In contrast, no grain-growth was observed during the 1 MeV electron irradiation of Zr–Fe thin-films. A bright-field image of the Zr–Fe foil irradiated at room temperature to 64 dpa is shown in Fig. 3 (top left). The grain size in the beam spot is the same as outside. This result indicates that isolated displacements such as created during electron irradiation do not induce grain-growth, at least in the low temperature regime where the irradiations were carried out. In other words, at low temperatures, grain-growth occurs only when irradiation induced cascades are involved. A model has been proposed to explain the kinetics of grain-growth under ion-irradiation where both the number of atomic jumps created within thermal spikes and the size of these thermal spikes play a crucial role on grain-growth [24].

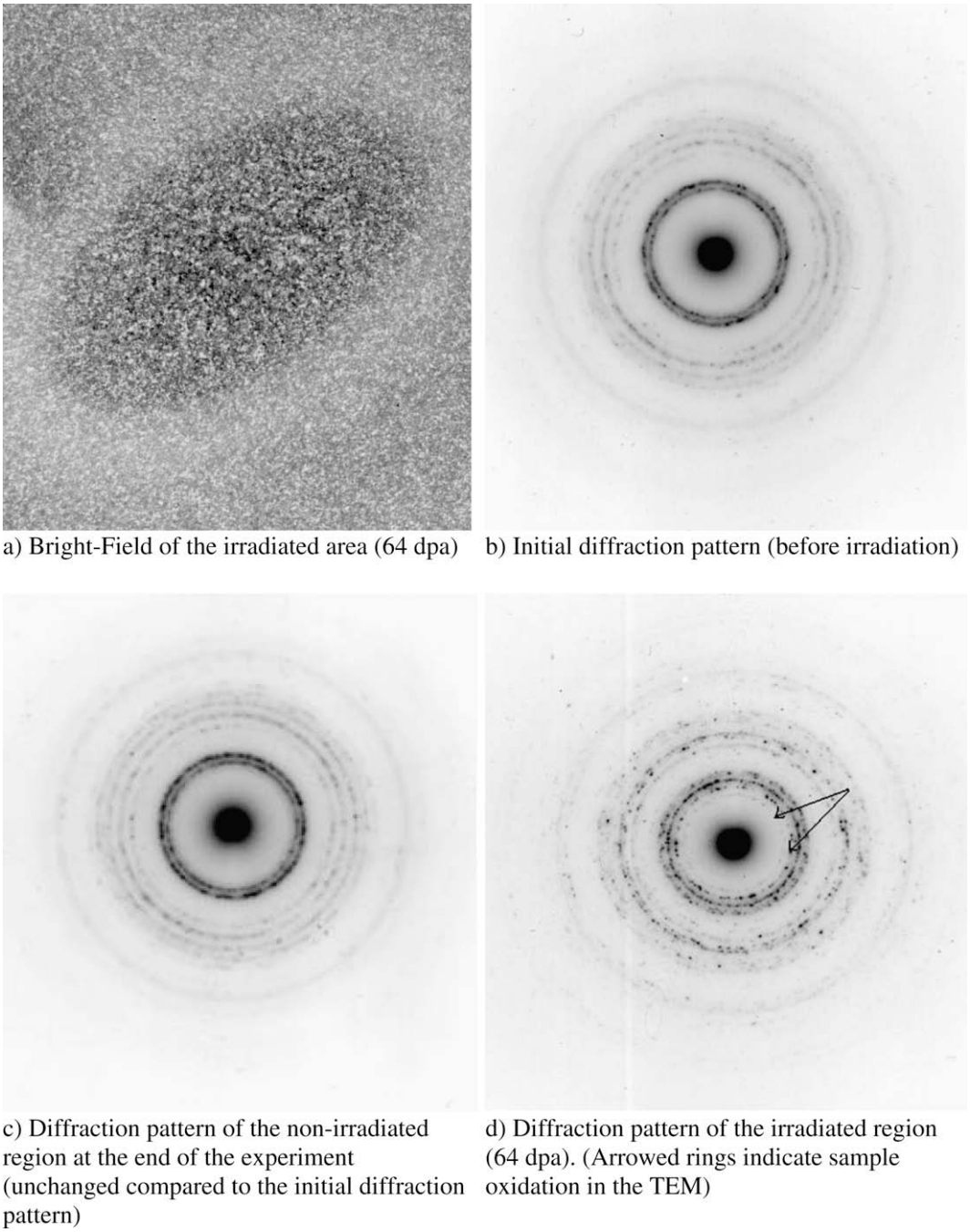

Fig. 3. Microstructure of the Zr–2%Fe thin-film irradiated at room temperature with 1 MeV electrons (*post mortem* analysis).

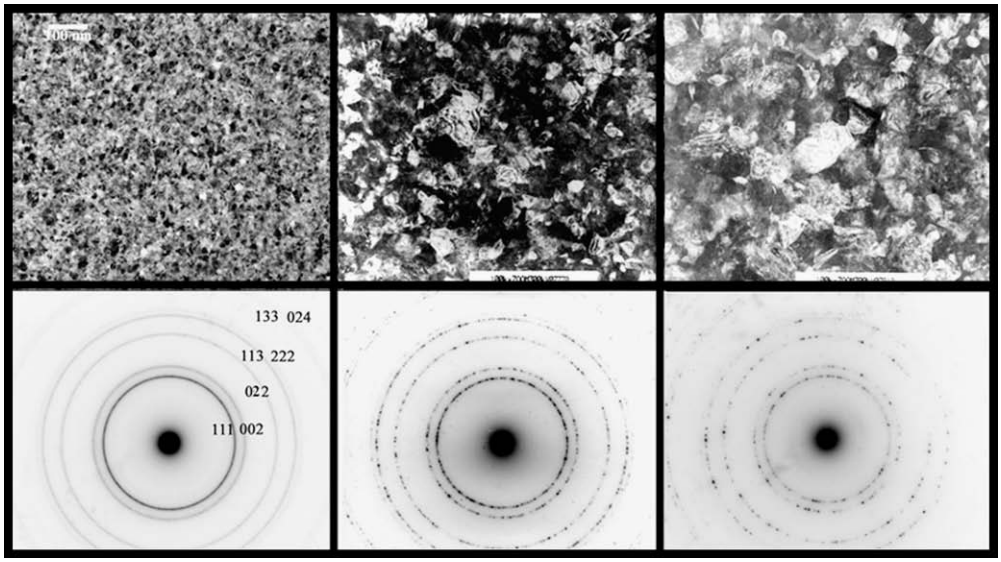

Fig. 4. Bright-field images and diffraction patterns of Cu(Fe) thin-films in the as-fabricated state (left), after 500 keV Kr irradiation to a final fluence of 10^{16} ions/cm^2, at 298 K (center), and 473 K (right), respectively.

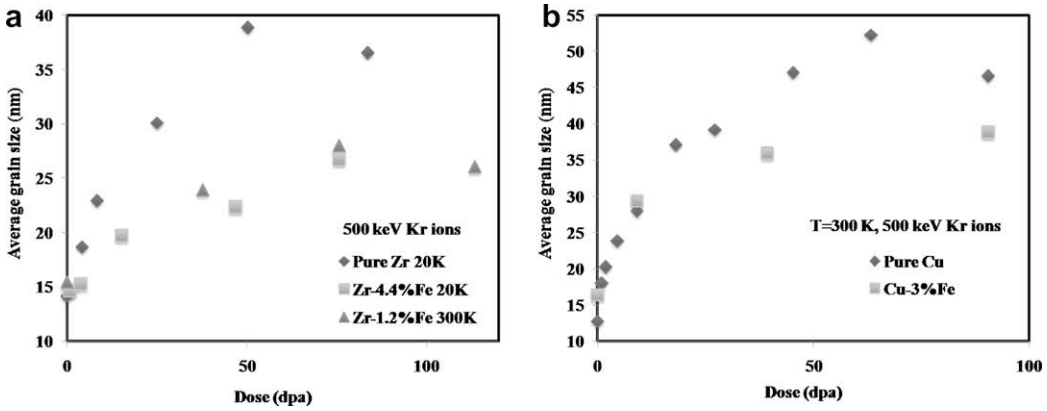

Fig. 5. (a) Average grain size in Zr, Zr–1.2%Fe, and Zr–4.4%Fe films irradiated in situ with 500 keV Kr ions plotted versus the dose in dpa. (b) Average grain size in Cu and Cu–3%Fe films irradiated in situ at room temperature with 500 keV Kr ions plotted versus the dose in dpa.

The effect of temperature on ion-irradiation induced grain-growth has been investigated in Zr–Fe [25] and Pt, Au, Cu thin-films [26] irradiated at temperatures varying from 20 K to 773 K. The studies demonstrated the existence of a low temperature regime where the kinetics of ion-irradiation induced grain-growth do not depend on the irradiation temperature indicating that the migration of the grain-boundary is controlled by intra-cascade ballistic processes in this regime (all the irradiations reported here are in the recombination dominated regime [24]). On the other hand, in the higher temperature range (above 0.14–0.22 T_{melt}), the dependence on irradiation temperature suggested that the expressions of the grain-boundary mobility and the grain-growth rate should include a temperature-dependent term.

The present study highlights the effect of alloying element on ion-beam induced grain-growth. The presence of Fe decreases the kinetics of grain-growth with respect to pure Zr and Cu thin-films, respectively. Fig. 5(a) shows the average grain size measured as a function of dose for pure Zr, for Zr–1.2%Fe and Zr–4.4%Fe foils irradiated with 500 keV Kr ions in the low temperature regime where grain-growth kinetics do not depend on the irradiating temperature. The supersaturated solid-solutions showed less ion-beam induced grain-growth than did pure Zr. Indeed the presence of the Fe alloying element slows down the initial grain-growth rate (slope of the curve at the origin) and results in smaller final average size. Solute drag and/or precipitate formation could be responsible. For the compositions studied, (1.2–4.4%Fe), no dependence of grain-growth with increasing Fe content was seen, suggesting that the lowest Fe contents used were enough to slow down grain-growth. Fig. 5(b) shows the average grain size for pure Cu and for Cu–3%Fe irradiated in the same conditions (at 300 K, with 500 keV Kr ions). The Fe-containing films showed slower grain-growth than seen in pure Cu films. However, since no second-phase precipitate could be detected in the diffraction patterns, it is likely that solute drag is the mechanism for slowing down the ion-irradiation induced grain-growth in the Cu–3%Fe thin-films. The fact that grain-growth is decreased by the addition of solute is most likely a result of solute drag or precipitate drag (when precipitation occurs as a result of irradiation). Also, it is possible that the presence of different atomic species within the thermal spikes may impact the spike size (focuson effect).

5. Conclusions

A study was performed of irradiation induced grain-growth in Zr, Cu and solid-solutions of Zr(Fe) and Cu(Fe) by exposing

free-standing thin-film samples to an ion-beam while observing grain-growth in a transmission electron microscope. The main conclusions are:

1. In both the Zr–Fe and Cu–Fe thin-films, grain-growth was decreased with respect to that observed in the pure Zr and Cu thin-films, respectively, likely a result of solute drag and precipitate drag (when precipitation occurs as a result of irradiation).
2. No grain-growth or second-phase precipitation occurred in the case of Zr–Fe irradiated with 1 MeV electrons at room temperature and 573 K, indicating that both processes require thermal spikes (as opposed to isolated defects).

Acknowledgements

The authors would like to thank the Materials Research Institute at Penn State, especially W. Drawl and L. Pillione for assistance with thin-film deposition, T. Van der Berghe, J. Perinet and I. Monnet at the CEA of Saclay for assistance during the electron irradiations performed, and A. Liu, E. Ryan, P. Baldo at Argonne National Laboratory for their assistance during the ion-irradiation experiments. The ion-irradiations were conducted in the IVEM-Accelerator facility at Argonne National Laboratory, which is supported as a User Facility by the US Department of Energy, Basic Energy Sciences, under contract W-31-109-ENG-38. This study was funded by DOE Nuclear Engineering Education Research program under Contract No. DOE-NEER (DE-FG07-01ID14115).

References

[1] R. Cauvin, G. Martin, J. Nucl. Mater. 83 (1) (1979) 67.
[2] P. Bellon, G. Martin, Phys. Rev. B 38 (4) (1988) 2570.
[3] G. Martin, Phys. Rev. B 30 (3) (1984) 1424.
[4] G. Martin, P. Bellon, F. Soisson, J. Nucl. Mater. 251 (1997) 86.
[5] D.E. Alexander, G.S. Was, J. Eridon, Nucl. Instrum. and Meth. B 39 (1989) 130.
[6] D.E. Alexander, G.S. Was, L.E. Rehn, Nucl. Instrum. and Meth. B 59&60 (1991) 462.
[7] H.A. Atwater, C.V. Thompson, H.I. Smith, J. Appl. Phys. 64 (1988) 2337.
[8] J.C. Liu, J. Li, J.W. Mayer, J. Appl. Phys. 67 (5) (1990) 2354.
[9] J.C. Liu, M. Nastasi, J.W. Mayer, J. Appl. Phys. 62 (2) (1987) 423.
[10] C.W. Allen, E.A. Ryan, Mater. Res. Soc. Symp. Proc. 439 (1997) 277.
[11] D. Kaoumi, A.T. Motta, R.C. Birtcher, Mater. Res. Soc. Symp. 908E (2005). Boston.
[12] R. Borrelly, P. Merle, L. Adami, J. Nucl. Mater. 170 (2) (1990) 147.
[13] G.M. Hood, J. Nucl. Mater. 159 (1988) 149.
[14] A.T. Motta, A. Paesano Jr., R.C. Birtcher, S.R. Teixeira, M.E. Bruckmann, L. Amaral, J. Appl. Phys. 85 (10) (1999) 7146.
[15] J. Ziegler, J.P. Biersack, U. Littmark, The Stopping and Range of Ions in Matter, Pergamon, New York, 1985.
[16] M. Griffiths, J. Nucl. Mater. 165 (1989) 315.
[17] A.T. Motta, D.R. Olander, A.J. Machiels, in: 14th International Symposium on the Effects of Irradiation on Materials, Andover, MA, June 1988, ASTM STP 1046, p. 457.
[18] D. Ariasand, J.P. Abriata, Bull. Alloy Phase Diagr. 9 (5) (1988) 597.
[19] K. Bhanumurthy, G.B. Kale, S.K. Khera, J. Nucl. Mater. 185 (1991) 208.
[20] Z. Altounian, C.A. Volkert, J.O. Strom-Olsen, J. Appl. Phys. 57 (6) (1984) 1777.
[21] A.T. Motta, L.M. Howe, P.R. Okamoto, J. Nucl. Mater. 270 (1999) 174.
[22] A.R. Miedema, Philips Tech. Rev. 36 (8) (1976) 217.
[23] A.M. Crespo-Sosa, M. Munoz, J.-C. Cheang-Wong, A. Oliver, J.M. Saniger, J.G. Banuelos, Mater. Sci. Eng. B 100 (3) (2003) 297.
[24] D. Kaoumi, A.T. Motta, R.C. Birtcher, J. Appl. Phys. 104 (1) (2008).
[25] D. Kaoumi, A.T. Motta, R.C. Birtcher, Nucl. Instrum. and Meth. B 242 (2005) 490.
[26] D. Kaoumi, A.T. Motta, R.C. Birtcher, J. ASTM Int. 4 (8) (2007) JAI100743.